Available online at www.sciencedirect.com
ScienceDirect
Trans. Nonferrous Met. Soc. China 35(2025) 2859−2873
Transactions of Nonferrous Metals Society of China
www.tnmsc.cn

Effects of flux purification on composition, microstructure and mechanical properties of Mg−9Li−3Al−1Zn alloy

Jia-wei SUN[1], Shi-hao XU[1], Yu-chuan HUANG[1], Lian-mei WU[2], Guo-hua WU[1], Wen-xia HU[2], Fei LI[2], Wen-cai LIU[1]

1. National Engineering Research Center of Light Alloy Net Forming and State Key Laboratory of Metal Matrix Composites, School of Materials Science and Engineering, Shanghai Jiao Tong University, Shanghai 200240, China;
2. Beijing Institute of Electronic System Engineering, Beijing 100854, China

Received 19 February 2024; accepted 7 January 2025

Abstract: The influence of refining flux composition, refining time, refining temperature, and addition amount on the microstructure and mechanical properties of Mg−9Li−3Al−1Zn alloy was investigated with orthogonal experimental design. The flux purification process for Mg−Li alloys was optimized and the most effective ternary flux composition was identified. Results indicate that flux purification significantly mitigates Li loss during smelting by forming a protective surface layer that reduces Li oxidation and evaporation. The optimal flux composition is LiCl:LiF:CaF_2 in a 3:1:2 mass ratio, with a flux addition of 3%, refining temperature of 720 °C, and holding time of 10 min. The elongation of alloy improves to 16.2% after refinement, while the enhancement in strength remains marginal.
Key words: Mg−Li alloys; flux purification; refining process; microstructure; mechanical properties

1 Introduction

Mg−Li alloys, recognized as one of the most lightweight structural materials, possess remarkable attributes such as high specific strength, exceptional specific stiffness, and excellent damping characteristics [1−3]. Unlike conventional Mg alloys with a hexagonal close-packed (HCP) crystal structure, Mg−Li alloys, particularly those with a high lithium content exceeding 6 wt.%, undergo a progressive transition to a body-centered cubic (BCC) structure, significantly enhancing the plasticity of alloy [4,5]. Consequently, owing to their exceptional properties, Mg−Li alloys have extensive utility in the aerospace, military, and consumer electronics industries [6−8].

Current research on Mg−Li alloys primarily addresses alloying, heat treatment, and thermoplastic processing issues, emphasizing synergistically enhancing the strength and plasticity of alloy. For instance, the incorporation of elements such as Al, Zn, and Ca substantially improves the strength of Mg−Li alloys [9−13]. Numerous studies have focused on the solid solution heat treatment of Mg−Li alloys [14−16]. Moreover, hot extrusion has demonstrated the potential to enhance the strength and plasticity of as-cast Mg−Li alloys [17,18]. However, practical industrial applications of Mg−Li alloys encounter primary challenges during the initial stages of melting and casting. Both Mg and Li are highly reactive elements, making the high-quality melting of Mg−Li alloys a critical and demanding issue in industrial production. Currently, vacuum induction melting serves as the predominant method employed for the melting and casting of Mg−Li alloys, effectively preventing oxidation and burn-off of the molten Mg−Li alloy. Nonetheless, this method exhibits drawbacks, such as the inability to degas and treat inclusions in the

Corresponding author: Wen-cai LIU, Tel: +86-21-54742630, Fax: +86-21-34202794, E-mail: liuwc@sjtu.edu.cn
https://doi.org/10.1016/S1003-6326(25)66853-1

molten state, resulting in reduced yields in actual production. Although direct melting in an atmospheric environment offers advantages in terms of cost and scalability, it presents significant challenges for molten metal protection and purification. Uncontrolled and intense combustion could occur at melting temperatures, leading to elevated inclusion content. Therefore, comprehensive exploration and research on the melting process of Mg−Li alloys, alongside the investigation of molten metal purification techniques, will significantly promote the further application and development of Mg−Li alloys [19].

To ensure the quality of the melt, the air melting process typically relies on the combined effects of gas protection and flux protection. Gas protection methods include reactive gas protection and inert gas protection. Reactive gases, including N_2, CO_2, SO_2, SF_6, and their mixtures, are employed in air melting. AARSTAD [20] examined the protective capabilities and surface film morphology of different gas mixtures. The study found that a mixture of 1 vol.% SF_6 + 99 vol.% CO_2 and 1 vol.% SO_2 + 99 vol.% CO_2 exhibited the most effective protective effect. For air melting of Mg alloys, a flux mixture primarily consisting of $MgCl_2$, KCl, MgO, and CaF_2 is commonly utilized. This method presents the lowest cost among various purification techniques and is currently widely adopted. However, research specifically targeting flux purification for Mg−Li alloys remains limited, and dedicated refining fluxes and mature melting techniques for Mg−Li alloys have yet to be developed. Traditional refining fluxes for Mg alloys are not only inefficient but also result in substantial loss of Li element in Mg−Li alloys. Hence, developing dedicated refining fluxes and purification processes for Mg−Li alloys offers significant potential, including recycling alloy waste, reducing resource waste and lowering industrial cost [21−24].

Dual-phase Mg−Li alloys (α-Mg and β-Li) have garnered widespread attention in recent years. Common alloying elements such as Al and Zn are usually added to provide solid solution strengthening effects. Therefore, the composition system in this study is based on the dual-phase Mg−9Li−3Al−1Zn alloy, employing air melting to develop a refining flux suitable for production conditions. The study aims to improve the flux's wetting and adsorption capacity on inclusions, thereby enhancing its refining effectiveness. The impact of flux refining on the microstructure and mechanical properties of Mg−Li alloys is thoroughly examined.

2 Experimental

2.1 Method

The orthogonal experimental design was used to investigate the effects of refining temperature, additive amount, holding time, and flux composition on the purification efficiency of Mg−9Li−3Al−1Zn alloy during metal mold casting. The casting process was as follows: all raw materials, the slag removal ladle, and flux were preheated in an oven at 200 °C for over 2 h. Mg blocks were heated in the furnace first, and once Mg was fully melted and the temperature reached 720 °C, pure Al was added. After Al had completely melted and the temperature decreased to 710 °C, pure Zn was added and allowed to stand for 1 min. When the melt temperature rose back to 720 °C, the flow rate of the protective gas was increased, and a cover flux was applied to the surface of the melt. At this point, Li blocks wrapped in Al foil were added, with additional cover flux prepared to be used as needed. When the temperature reached 670−680 °C, heating was turned off. At the designed temperature, the refining flux was introduced in portions, with 1/4 to 1/3 of the total amount being sprinkled in first, followed by stirring. After all the refining fluxes were added, the melt was stirred thoroughly for 1 min before being left to stand. During the refining process, surface slag was skimmed off, and if stirring and skimming disturbed the surface, a small amount of cover flux was added. After refining, the melt was left to stand, and the temperature was then raised to 720 °C to ensure sufficient fluidity for casting.

The current refining process is as follows: the additive amount of flux is 3 wt.% of the melt, the refining temperature is 700 °C, and the holding time is 20 min. However, the high content of CaF_2 in the existing refining flux increases viscosity and reduces spreading capability, which can decrease the purification effect. Therefore, a reduction in the CaF_2 content was deemed necessary in the refining flux. Based on the aforementioned process and the composition of the flux, three levels were selected

for each factor, as shown in Tables 1 and 2. Among them, three levels of flux types (A, B, and C) differ only in the CaF_2 content.

In this study, the recognized Taguchi orthogonal array was used. An orthogonal experimental design was chosen due to its ability to facilitate an effective and systematic evaluation of multiple factors and their interactions, which is crucial for optimizing the refining and purification process. This method significantly reduces the number of experiments required while providing comprehensive insights into the effects of various parameters. According to the design criteria, the L9 (3^4) orthogonal array was selected, and the DoE orthogonal design was conducted using Minitab to obtain the experimental orthogonal array. The nine group tests are named as Test 1−9. Test 0 is the control group.

Table 1 Composition and proportion of each flux

Flux	Mass ratio	$w(CaF_2)$/%
A	LiCl:LiF:CaF_2=3:1:1	20.0
B	LiCl:LiF:CaF_2=3:1:2	33.3
C	LiCl:LiF:CaF_2=3:1:3	42.9

Table 2 Different factors and levels for orthogonal experiment

Flux	Level	Content/wt.%	Temperature/°C	Time/min
A	1	2	680	10
B	2	3	700	20
C	3	4	720	30

2.2 Characterization

The actual chemical composition of the tested materials was determined through Inductively Coupled Plasma-Atomic Emission Spectrometry (ICP-AES, Avio 500). All samples were extracted from the bottom of the plate-shaped ingot at a height of 10 mm from the bottom up, ensuring the sampling locations were far from the surface and the riser of the ingot to avoid inclusions and other defects, as shown in Fig. 1(a). Vickers hardness was tested using the XHVT-10Z hardness tester, employing a 5 kg load for 15 s and at least 10 hardness measurements were conducted for each sample. Tensile properties were assessed using dog-bone-shaped specimens, characterized by a gauge length of 15 mm and cross-section of 3.5 mm × 2 mm, as shown in Fig. 1(b). Each test was performed at least 3 times, and all experiments were conducted using Zwick/Roell Z100 machine with strain speed of 1 mm/min at room temperature. The alloys were mechanically polished and chemically etched using a 4 vol.% nitrate ethanol solution. Microstructural observation and analysis were accomplished by optical microscopy (OM, Zeiss Axioscope 5) and scanning electron microscopy (SEM, Phenom XL) equipped with energy-dispersive X-ray spectroscopy (EDS). X-ray diffraction (XRD, Bruker D8 ADVANCE) was conducted at a scanning speed of 4 (°)/min using Cu K_α radiation, with step size of 0.02° for phase analysis.

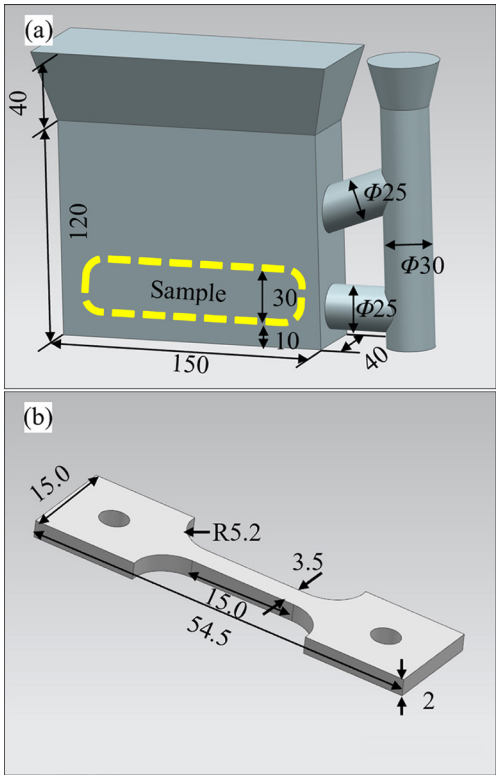

Fig. 1 Schematic diagram of ingot and sample: (a) Ingot dimension and sampling location; (b) Dimension diagram of tensile test sample (Unit: mm)

3 Results

3.1 Effect of flux purification on composition and inclusions of Mg−Li alloys

The measured chemical composition of the Mg−Li alloy is presented in Table 3. It can be observed that there is minimal deviation in the content of non-matrix elements such as Al and Zn between the flux-free control group (Test 0) and the

Table 3 Chemical compositions of Mg−9Li−3Al−1Zn alloy (wt.%)

Test No.	Li	Al	Zn	Mg
0	8.39	3.12	1.09	Bal.
1	8.82	3.09	1.03	Bal.
2	8.83	3.01	0.98	Bal.
3	8.79	2.96	0.98	Bal.
4	9.03	2.96	1.09	Bal.
5	8.92	2.99	1.04	Bal.
6	8.86	2.93	0.96	Bal.
7	9.12	2.91	1.02	Bal.
8	9.08	2.92	0.91	Bal.
9	8.87	2.97	1.00	Bal.

various experimental groups. The primary deviations are concentrated in the mass fraction of Li, particularly with the control group exhibiting significantly lower Li content compared with any of the experimental groups. This suggests that flux purification has a noticeable impact on the Li content in the Mg−Li alloy and can enhance its Li content. This is attributed to the presence of Li salts, such as LiCl and LiF, in the refined flux. These salts undergo partial decomposition, generating Li and Cl_2 at elevated temperatures (>600 °C), thus supplementing the Li element in the melt to a certain extent. Additionally, after melting, the refined flux may contain liquid flux and aggregated impurities that form a flux-oxide composite surface layer, isolating the external air and reducing the evaporation and oxidation loss of Li.

In Table 3, the elemental content in the experimental groups numbered 1−9 is consistent with the designed composition. This implies that different refining processes and refined fluxes have a negligible effect on the Li content. The Li content remains stable at approximately 9 wt.%, indicating that when using LiCl−LiF−CaF_2-based refining flux, variations in the refining process and flux component proportions, when within a reasonable range, do not significantly affect the chemical composition of alloy. Therefore, the adoption of refining flux purification processes will influence the alloy's composition, reducing the loss of Li and thereby stabilizing the chemical composition of the Mg−Li alloy.

Quantitative metallographic analysis of the metallographic samples was conducted using Image Pro Plus (IPP) image analysis software. Thirty statistical field areas are randomly selected, and the software directly outputs the area fraction of inclusions, distinguished by color, shape, and SEM composition analysis. This area fraction is used as the average inclusion content.

The statistical results from Fig. 2 indicate that the total inclusion content in the flux-free control group is higher than that in any experimental group, demonstrating that flux purification has a substantial effect on purifying Mg−9Li−3Al−1Zn alloys. This process effectively enhances melt purity and reduces inclusion content. Additionally, the statistical results show that after flux purification, the number of large particles (size >50 μm) decreases, and the inclusion particle size is less than 20 μm, further confirming the effectiveness of flux purification.

Based on the above analysis, it is concluded that flux composition primarily affects the total inclusion content. An optimal flux composition significantly reduces the total inclusion content. In contrast, refining temperature primarily affects the size distribution of inclusions. Higher refining temperatures increase the proportion of small particle inclusions and reduce the number of large particle inclusions. As the most direct indicator of purification effectiveness, the inclusion content is most significantly influenced by flux composition (i.e., CaF_2 content). Therefore, identifying the most suitable flux composition is the most cost-effective and direct way to enhance purification effectiveness.

3.2 Effect of flux purification on microstructure and mechanical properties of Mg−Li alloy

Figure 3 displays the metallographic microstructure of the Mg−Li alloy. The bright gray phase corresponds to the α-Mg phase, which is a solid solution of Li in Mg. The dark gray phase represents the β-Li phase. For Mg−Li alloy, when the Li content ranges from 5.7 to 10.3 wt.%, the matrix phase of the alloy consists of α-Mg and β-Li phases. Furthermore, the β-Li phase increases with the increase in Li content, consistent with the observations in the metallographic photograph. In addition, it is noticeable that there are a small number of dispersed second-phase particles distributed at grain boundaries or phase boundaries. Moreover, in all the metallographic images, there are granular or blocky inclusions.

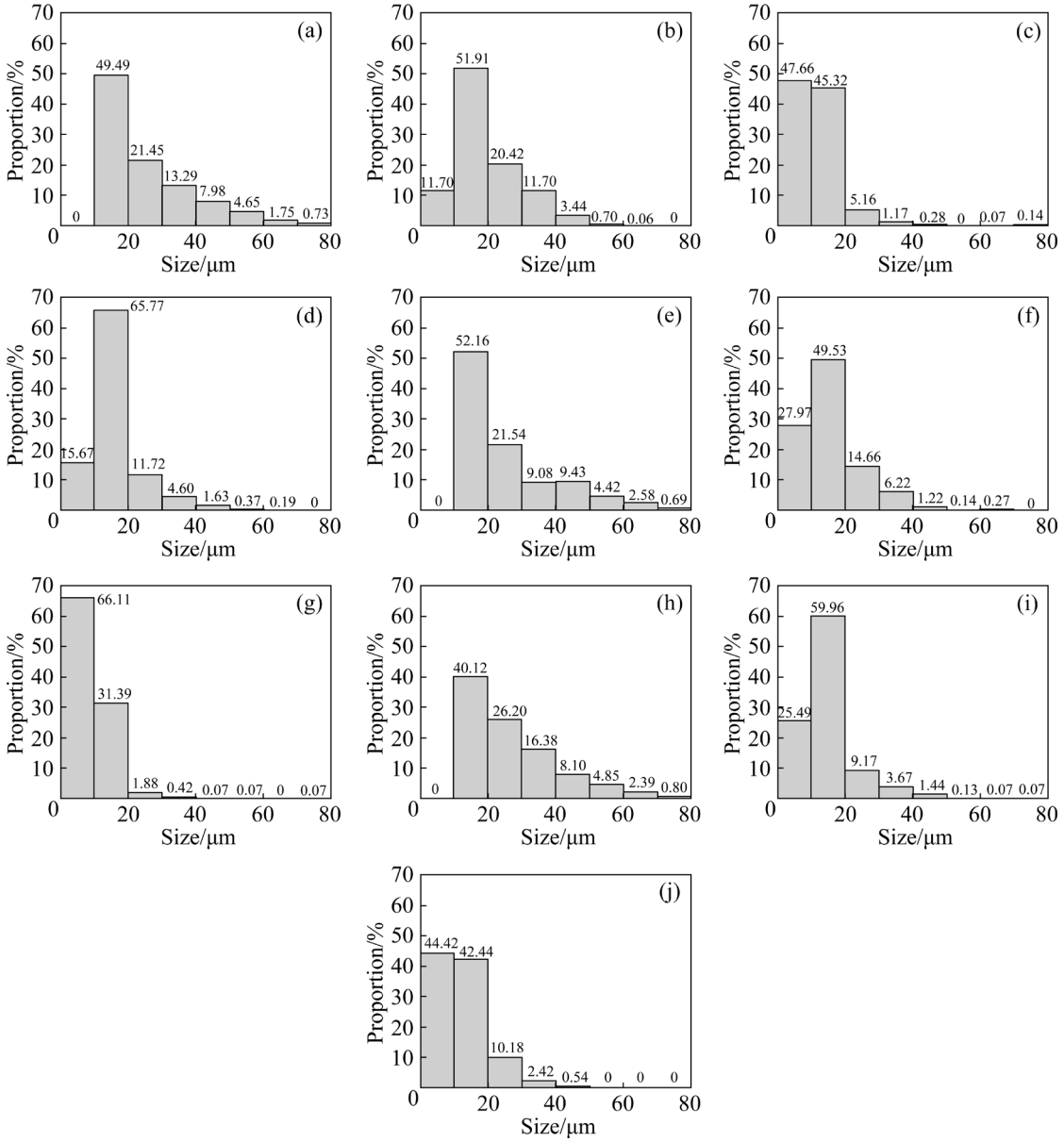

Fig. 2 Statistical histograms of inclusion distribution and particle size: (a) Test 0; (b)Test 1; (c) Test 2; (d) Test 3; (e) Test 4; (f) Test 5; (g) Test 6; (h) Test 7; (i) Test 8; (j) Test 9

In Fig. 3(a), this alloy represents the flux-free control group, and its metallographic image reveals the presence of numerous inclusions with relatively coarse sizes. This demonstrates the effectiveness of flux in impurity removal and purification. A comparison of the metallographic images of different alloy groups reveals that the primary differences lie in the content and size distribution of inclusions, whereas the matrix and distribution of secondary phases remain largely unchanged. Thus, with the refining process primarily affecting the content and distribution of inclusions and exerting little influence on the constituent phases.

The metallographic images indicate that the flux purification scheme for Test 6 is the most favorable, as shown in Fig. 3(g). It exhibits the least amount of inclusions, and the size of the inclusions is also the smallest, with no prominent large particle inclusions visible. The density, viscosity, wettability, and surface tension of the flux are suitable, ensuring thorough encapsulation and settling of the inclusions. The amount of flux is adequate to fully encapsulate the inclusions without forming flux inclusions in the melt. Additionally, the settling time for this process is the shortest, resulting in minimal oxidation of the melt during the settling period, thus preventing the formation of new inclusions or only producing a small number of small-

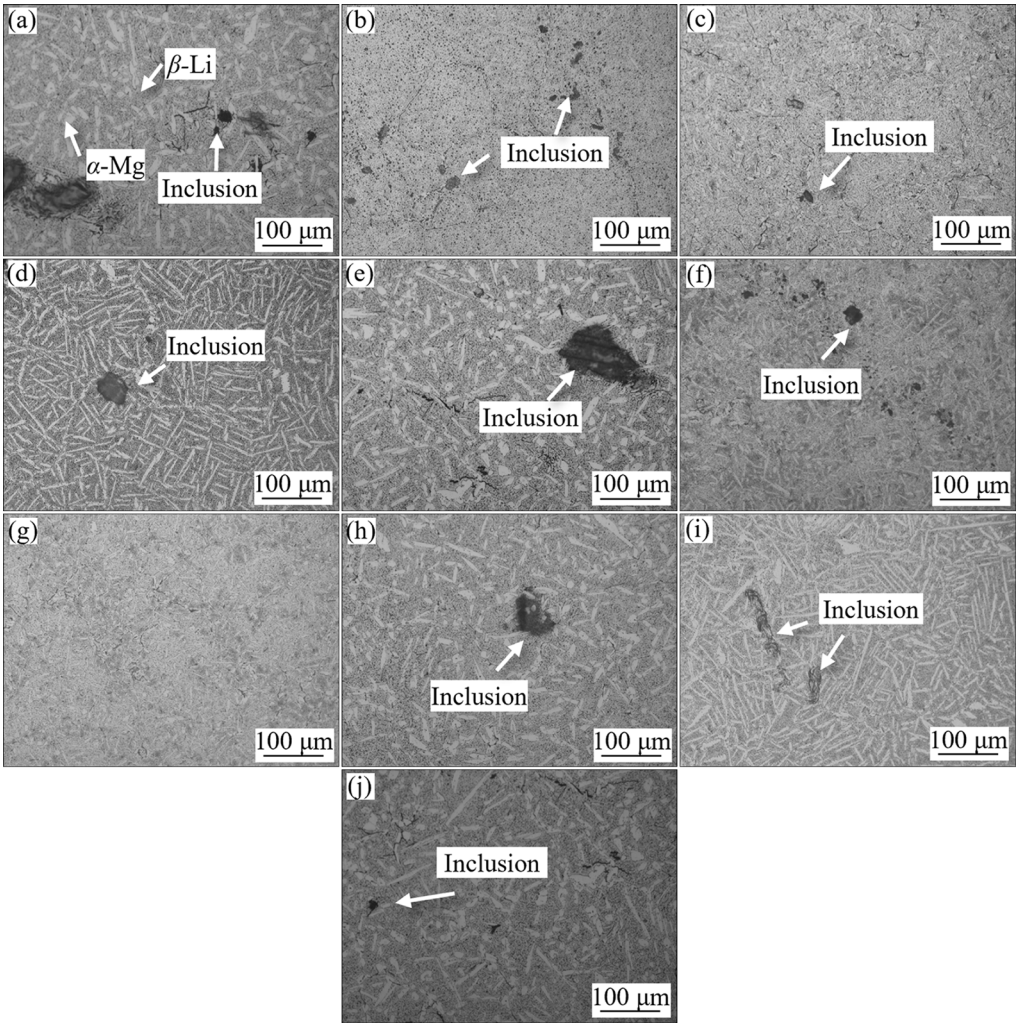

Fig. 3 Metallographic structures of Mg−Li alloy: (a) Test 0; (b)Test 1; (c) Test 2; (d) Test 3; (e) Test 4; (f) Test 5; (g) Test 6; (h) Test 7; (i) Test 8; (j) Test 9

sized inclusions. On the other hand, the flux purification effect for Test 4 is relatively poor, with a high overall inclusion content and several large particle inclusions, as shown in Fig. 3(e). This could be attributed to the highest content of CaF_2 in the refining flux and the lowest refining temperature. The high melting point of CaF_2 leads to insufficient dispersion or inadequate wetting of the flux in the melt, preventing sufficient coverage of the inclusions. Moreover, the longer settling time allows continued oxidation of the melt, further compromising the purification effect and resulting in the presence of large particle inclusions in the microstructure.

The most significant inclusions in Mg−Li alloys are oxide inclusions [25]. Typical oxide inclusion morphologies in the alloy were captured using SEM. EDS analysis was employed for elemental analysis, as shown in Fig. 4 and Table 4. Most oxide inclusions consist of a mixture of MgO and Li_2O. As the EDS equipment cannot characterize Li element, only Mg is labeled in the image.

Figure 5 shows the typical inclusion morphologies and EDS analysis results of Mg−Li alloys, excluding oxide inclusions. The analysis reveals that common inclusions found in the experimental Mg−Li alloys include carbides, carbon oxides, flux inclusions, and mixtures. As shown in Fig. 5(a), the EDS mapping results indicate that the analyzed inclusion belongs to carbide inclusions, which are primarily in the form of particles or blocks and constitute a significant portion of the inclusions. The presence of these inclusions may be attributed to the reduction of CO_2 in the protective gas or air by Li, as well as the use

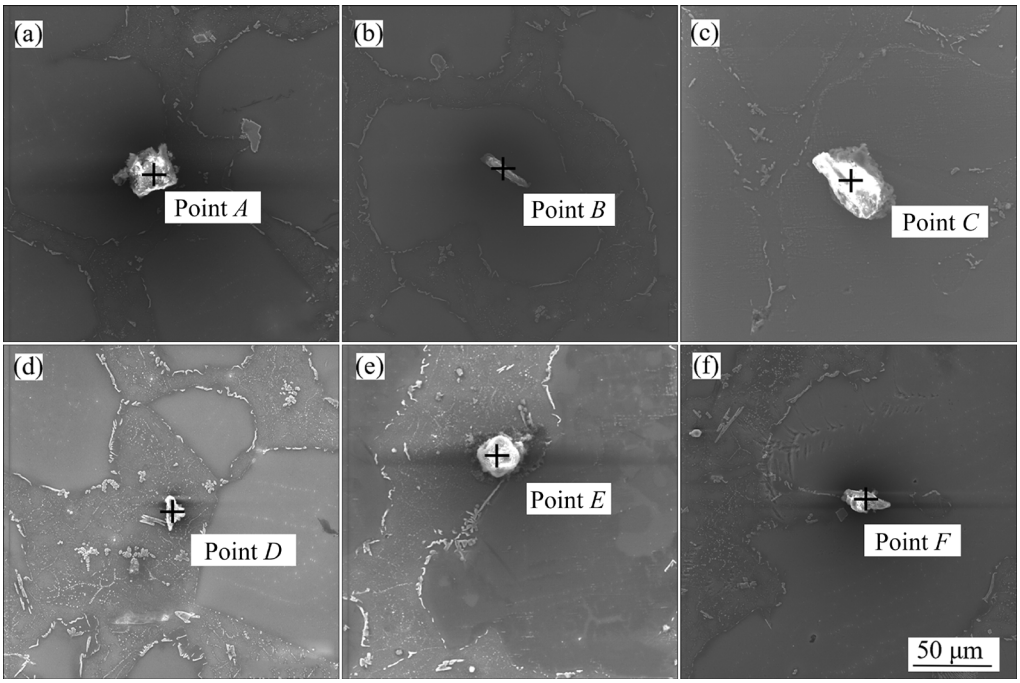

Fig. 4 SEM images of typical oxide inclusions: (a) Cube; (b) Rod; (c) Block; (d) Irregular shape; (e) Sphericity; (f) Taper

Table 4 EDS point analysis results of Fig. 4 (at.%)

Point	Mg	O
A	57.59	42.41
B	66.97	33.03
C	66.53	33.47
D	66.62	33.38
E	51.24	48.76
F	55.84	44.16

of graphite crucibles during melting, which could be one of the sources of carbide inclusions. The EDS result in Fig. 5(b) reveals the presence of Cl in the inclusion, indicating the contribution of residual LiCl from the flux. This suggests that some of the particulate or blocky inclusions are mixtures of carbide and flux inclusions. Figure 5(c) represents the typical morphology of CO_2 inclusions, which are generally small and in the form of particles. Figure 5(d) displays typical flux inclusions, characterized by large sizes (diameter >50 μm) and a flocculent structure. They mainly originate from residual flux, and their presence severely compromises the mechanical properties of the alloy.

Based on the previous analysis, three different Mg−Li alloys melted with different fluxes were selected for XRD diffraction analysis, as shown in Fig. 6. Regardless of the flux type, the main phases in the alloy are still α-Mg + β-Li, with a small number of secondary phases. The positions and intensities of the diffraction peaks are consistent across the alloys, indicating no significant differences in phase composition. This observation aligns with the trend shown in Fig. 3, suggesting that changes in the refining process or flux affect only the inclusion content and distribution, not the phase composition. The secondary phases in the Mg−9Li−3Al−1Zn alloy consist primarily of two types: metastable $MgLi_2Al$ and thermodynamically stable AlLi phase. The AlLi phase is formed through the decomposition of the metastable $MgLi_2Al$ phase and the direct combination of Al and Li atoms. The absence of Zn-containing phases in the XRD patterns is because Zn primarily exists in the form of a solid solution within the matrix alloy phase. In contrast, Al-containing precipitate phases are more easily formed.

Figure 7 shows the Vickers hardness of the as-cast Mg−Li alloys in the control group and experimental groups. It can be observed that the hardness of all alloys fluctuates around HV 70, and there is no significant difference between the control group without refining and the various experimental groups. This reveals that refining has

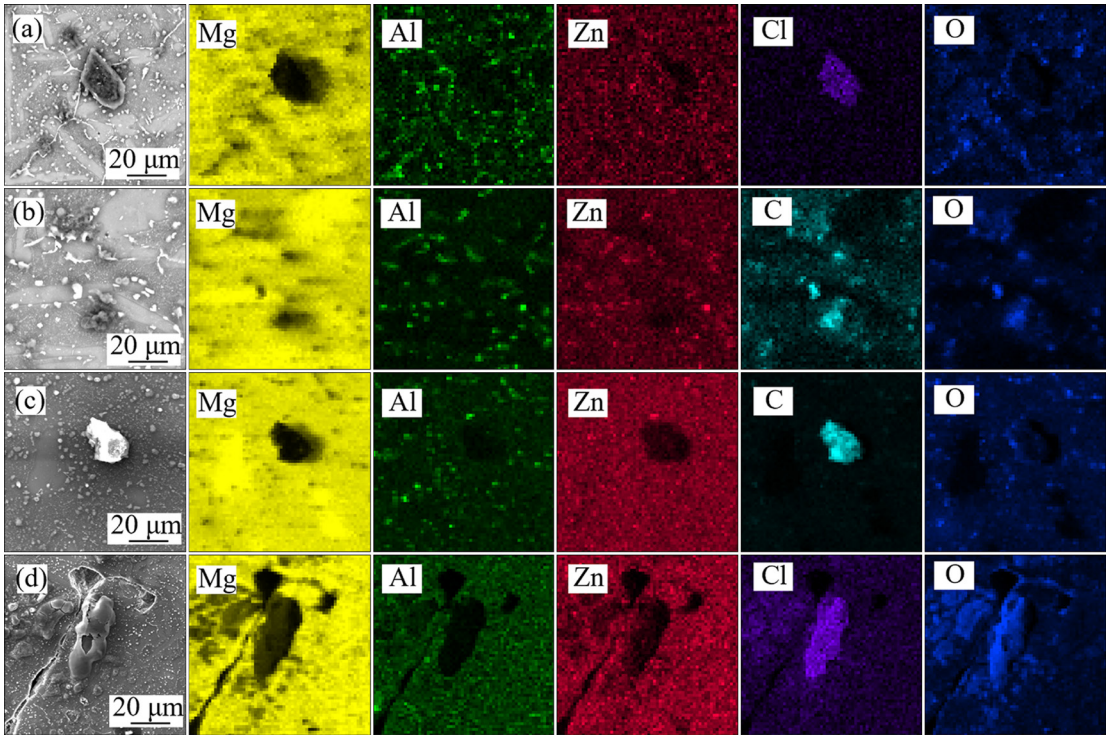

Fig. 5 SEM images and EDS surface scanning of inclusions: (a) Carbide inclusion; (b) Carbide inclusion mixture with flux; (c) Carbonic oxide inclusion; (d) Flux inclusion

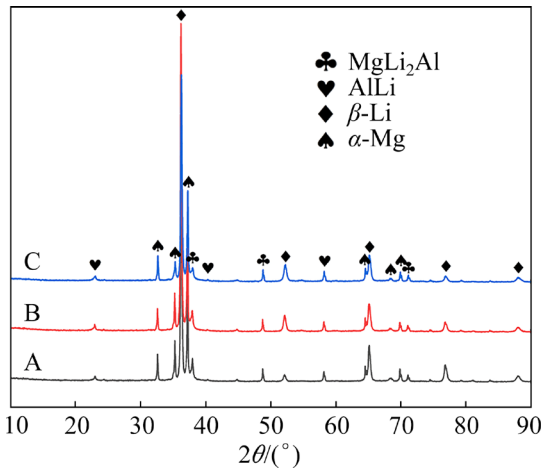

Fig. 6 XRD patterns of Mg−Li alloys refined with three fluxes A, B and C

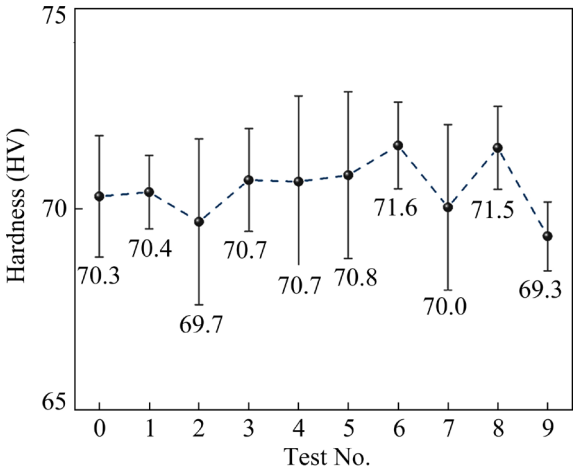

Fig. 7 Hardness (HV) of different Mg−9Li−3Al−1Zn alloys

no significant effect on the hardness of the alloy, and differences in refining processes have minimal impact. Therefore, it can be concluded that the hardness of the alloy cannot be improved through the purification of the melt.

Tensile tests were conducted on each specimen, and the stress−strain curves were plotted as shown in Figs. 8(a, b). The data for each alloy group are presented in Fig. 8(c). A comparison of the 10 stress−strain curves and the data in Fig. 8(c) shows that the main difference in the mechanical properties of the as-cast alloys lies in elongation (EL), while the differences in yield strength (YS) and ultimate tensile strength (UTS) are minimal. This is likely because yield strength is primarily determined by material composition. When inclusion content does not significantly affect mechanical properties, Mg−Li alloys with similar compositions will not show distinct differences in yield strength. When inclusions do not impair the

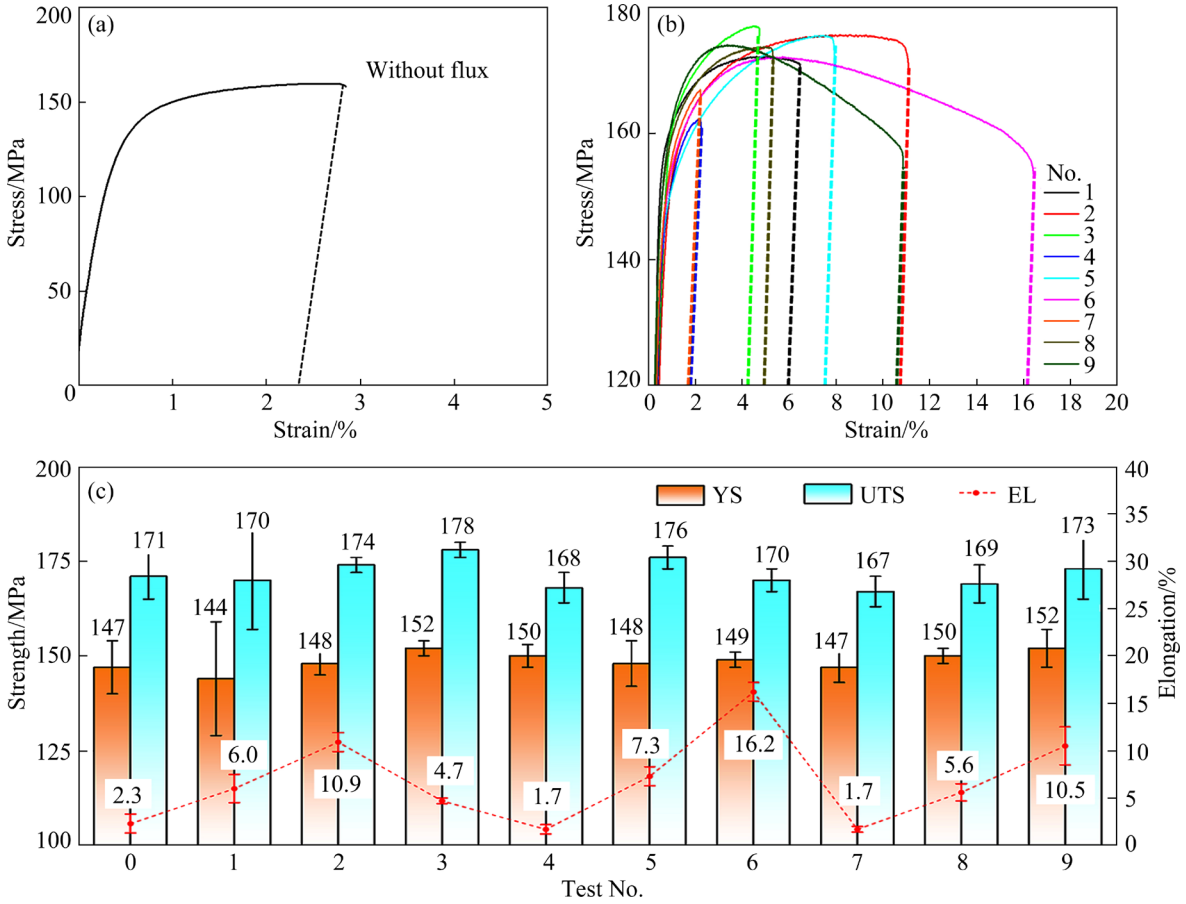

Fig. 8 Tensile test results of Mg−9Li−3Al−1Zn alloy: (a) Stress−strain curves without flux; (b) Stress−strain curves of experimental groups; (c) Mechanical properties

mechanical properties of alloy, the difference in ultimate tensile strength remains minimal. It is well known that high-lithium-content Mg−Li alloys, unlike conventional Mg alloys, have a higher yield-to-tensile strength ratio, which also indicates a lower level of work hardening capacity. Although flux purification reduces inclusions in the Mg−Li melt, minimizing crack initiation and propagation, it does not substantially enhance the strength of material. Elongation is primarily determined by the plasticity of material, with grain boundaries, phase boundaries, and inclusion/matrix interfaces generally exhibiting lower strength. Stress concentration phenomena in these regions make them prone to crack initiation, and cracks tend to propagate along the interface between inclusions and the matrix, resulting in differences in elongation associated with different inclusion contents at the macroscopic level [26].

The previous discussion highlighted that the inclusion content and distribution are influenced by four factors: the amount of added flux, refining temperature, holding time, and flux composition. Consequently, these factors also affect the mechanical properties of the alloy. A main effects plot illustrating the relationship between these factors and the mechanical properties is shown in Fig. 9. According to Fig. 9(a), mean of YS gradually increases with both the flux amount and refining temperature. The YS initially rises with holding time, but then decreases, showing a trend similar to that of flux amount. Figure 9(b) reveals a negative correlation between the flux amount and mean of UTS, while the refining temperature and holding time have a promoting effect on the UTS. The influence of flux composition on UTS fluctuates, with an initial decrease in UTS followed by an increase as CaF_2 content rises. Given the relatively smooth fluctuations in yield strength and UTS, the focus shifts to elongation. For the plasticity of the alloy, the increase of flux amount and CaF_2 content result in an improvement in mean of elongation, followed by a decrease. This suggests that both additions promote elongation in some

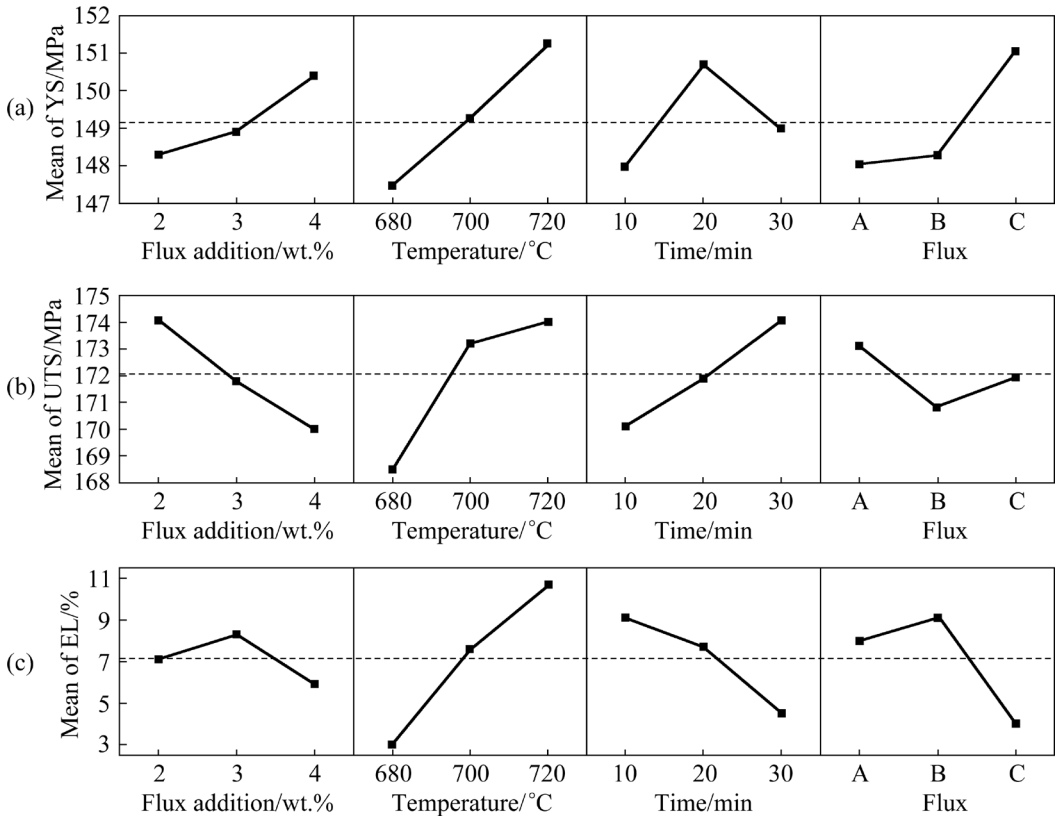

Fig. 9 Effect of experimental factors on mechanical properties: (a) YS; (b) UTS; (c) EL

extent. Excessive flux addition, however, can lead to flux inclusions in the ingot, impairing the plasticity of alloy. When the CaF_2 content is excessively high, the flux becomes viscous and dense, making it difficult for inclusions to adequately aggregate during the refining process, thereby compromising the refining effectiveness.

Moreover, increasing the refining temperature enhances the elongation of the alloy. This can be attributed to the high temperature of the melt, which improves the viscosity of the refining flux, facilitating the aggregation of inclusions and reducing the overall inclusion content. In contrast, longer holding time corresponds to lower elongation, indicating that extended holding impairs melt purification. During the holding process, the melt continuously undergoes oxidation, increasing the size and number of oxide inclusions. As a result, these inclusions are prone to initiating cracks during tensile testing, leading to rapid fracture once the alloy reaches UTS.

To investigate the significant influence of refining temperature on elongation, the tensile fracture surfaces of the Mg−9Li−3Al−1Zn alloy at different refining temperatures were observed, as shown in Fig. 10. Figures 10(a−d) show that the fracture surfaces exhibit numerous pits and tearing edges, typical characteristics of plastic fracture in Mg−Li alloys. Noticeable cleavage structures are also observed, indicating brittle fracture features. The Mg−9Li−3Al−1Zn alloy is a dual-phase alloy consisting of hcp structures (α-Mg) with limited slip systems and bcc structures (β-Li) with more slip systems. Based on the phase diagram and metallographic observations, α-Mg is relatively scarce, while β-Li is more abundant. Thus, fracture surfaces exhibit small, deep dimples. Large inclusions and second-phase particles are found in the dimples, while fine second-phase particles and inclusions are rarely observed near the cleavage planes. This is because the second-phase particles, such as $MgLi_2Al$ or AlLi, tend to concentrate at the phase boundaries and within the β-Li phase. During the slip process, the second-phase particles or inclusions, subjected to compression, move with the β-Li phase, resulting in the concentration of the second-phase particles or inclusions at the β-Li phase, ultimately appearing predominantly near the dimples on the fracture surface.

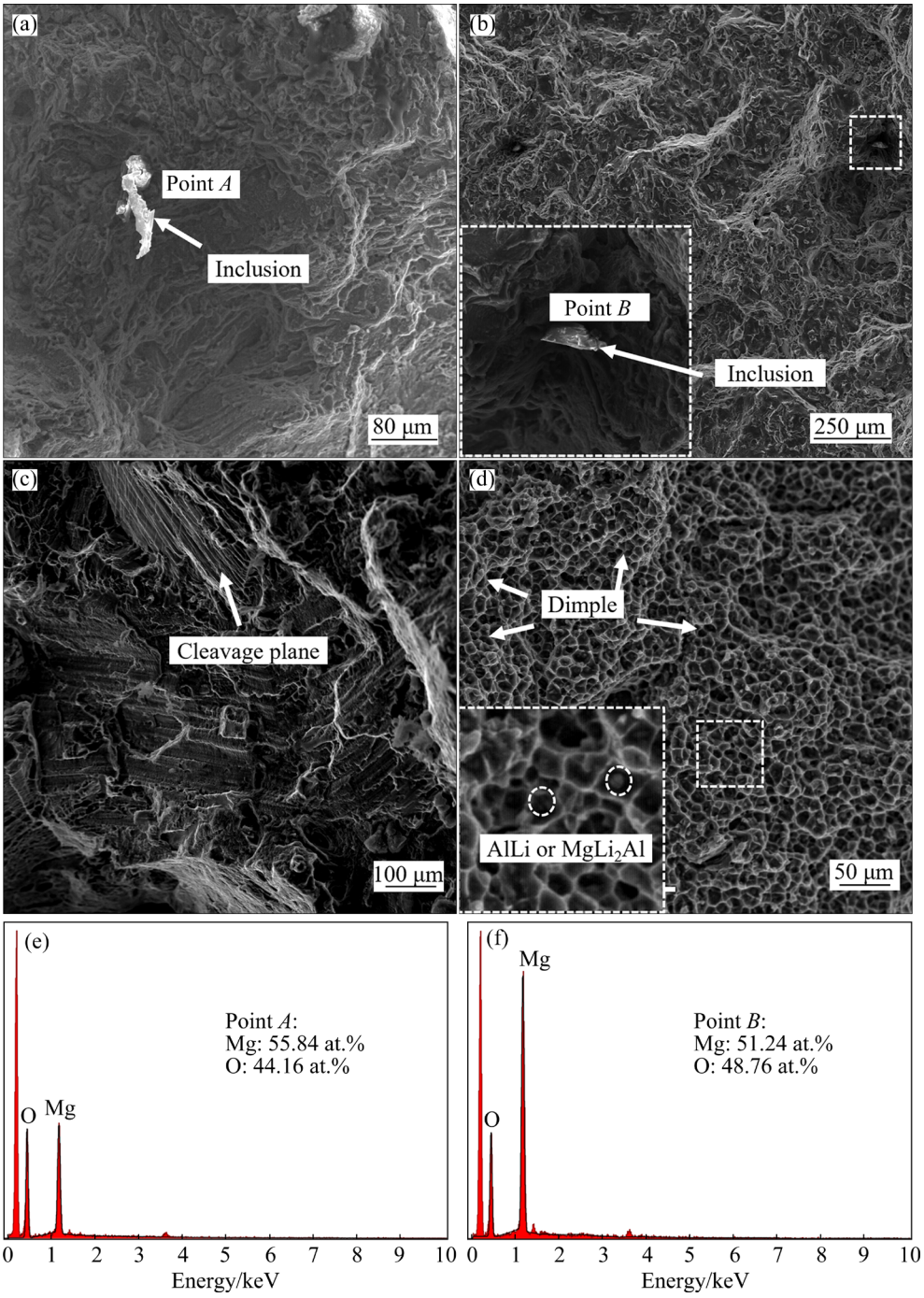

Fig. 10 SEM images showing tensile fracture of Mg−9Li−3Al−1Zn alloy (a−d), and corresponding EDS analysis of Points *A* and *B* (e, f): (a) Without flux, Test 0; (b) 680 °C, Test 4; (c) 700 °C, Test 5; (d) 720 °C, Test 6

4 Discussion

The effects of the experimental factors on purification effectiveness are shown in Fig. 11. The proportion of small particle inclusions (particle size <10 μm) initially increases and then decreases as the amount of flux is increased. This suggests that merely increasing the amount of refining flux does not increase the quantity of small particle inclusions. This may be attributed to the formation of new inclusions by the refining flux, which reduces melt purity and increases the average inclusion size. Increasing the refining temperature from 680 to 720 °C results in a continuous increase in the proportion of small particle inclusions (<10 μm).

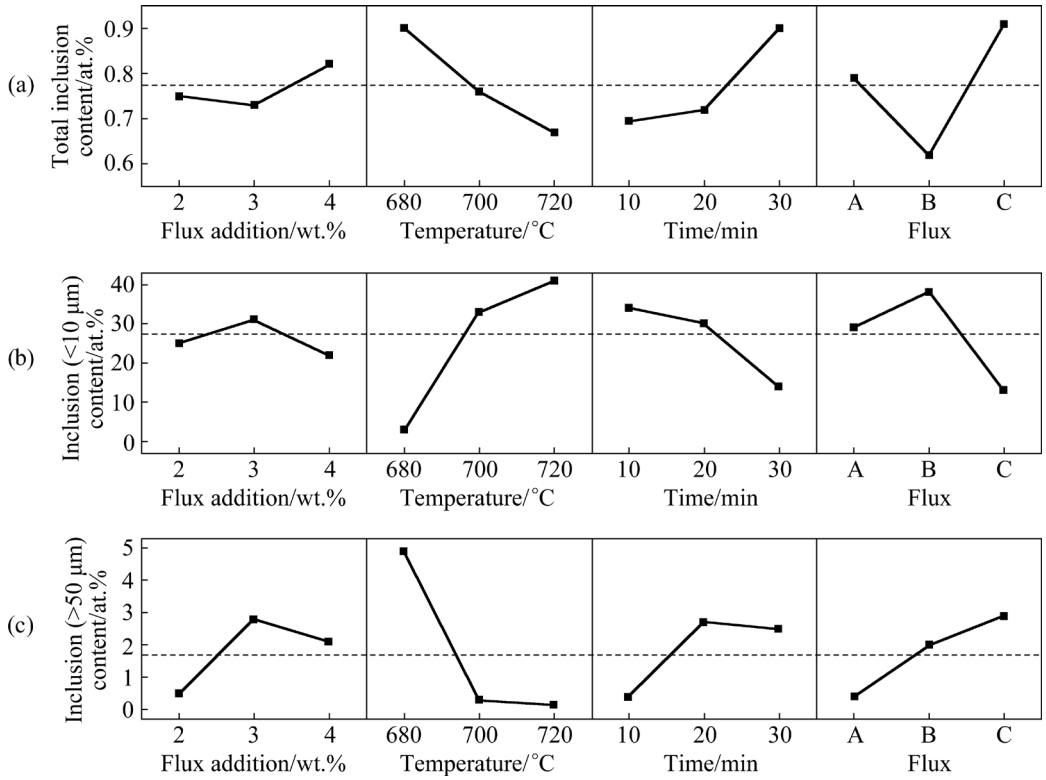

Fig. 11 Effect of experimental factors on purification: (a) Total inclusion content; (b) Inclusion (<10 μm) content; (c) Inclusion (>50 μm) content

This indicates that the refining temperature is an important factor influencing the performance of the refining flux. Higher refining temperatures improve the refining wetting ability of flux and facilitate the aggregation and settling of larger particle inclusions at the bottom of the melt.

As the holding time increases from 10 to 30 min, the proportion of small particle inclusions (particle size <10 μm) continuously decreases. This suggests that longer holding time results in an increase both in the number and size of inclusions. This can be attributed to defects in the surface oxide layer, which retain small amounts of air as evaporation channels for Li element, leading to the formation of more oxidized inclusions and a trend toward aggregation. Additionally, increasing the CaF_2 content in the refining flux initially increases the proportion of small particle inclusions but later causes it to decrease. This indicates that high viscosity in the liquid refining flux is not always advantageous, as excessive viscosity impairs the wetting of inclusions. Furthermore, high CaF_2 content increases the density of the refining flux, accelerating the settling rate and preventing complete coverage and settling of some particulate inclusions. Conversely, reducing the CaF_2 content leads to insufficient viscosity and density, hindering the aggregation and settling of inclusions and compromising purification effectiveness.

The main effect analysis of Fig. 11(c) shows that as the amount of flux increases, the proportion of large particle inclusions (>50 μm) initially rises and then declines. However, even at high flux addition levels, the proportion of large particle inclusions remains greater than that at the minimum addition level. This suggests that increasing the amount of flux may enhance purification to some extent, and it can also compromise effectiveness. Unconsumed flux can combine with inclusions to form large particles, ultimately lowering ingot quality.

Increasing the refining temperature decreases large particle inclusions but raising it beyond 700 °C has minimal effect. The effect of refining temperature on total inclusion content and small particle inclusions suggests that higher temperatures reduce inclusion content and increase small particle proportions.

As the holding time extends, the content of large particle inclusions initially increases and then

decreases but remains higher than that at the shortest holding time. Prolonged holding time increases the settling of large particle inclusions, but also leads to more inclusions and larger particle size.

Increasing the CaF_2 content leads to an increase of large particle inclusions. This suggests that high CaF_2 content increases the density, viscosity, and melting point of the flux, but is insufficient to fully settle large particles, limiting the purification effect.

The influence of refining temperature on inclusion content is second only to the flux composition and is a key factor affecting the size and distribution of inclusions. This indicates that the refining temperature determines the viscosity and fluidity of the molten salt, thereby influencing the purification behavior of the flux. The dynamic viscosity of the liquid flux can be expressed as follows [27]:

$$\eta = A\exp[Q/(RT)] \quad (1)$$

where A represents a constant; Q denotes the activation energy of viscosity; R is the molar gas constant; T represents the thermodynamic temperature.

According to Eq. (1), as the working temperature increases, the viscosity of the molten salt decreases. Consequently, the droplet size of the molten salt in the melt decreases, and the contact area between the flux and the melt increases, improving the purification efficiency of the flux. Furthermore, the decrease in viscosity enhances the coalescence effect of the droplets in the molten salt, facilitating the separation of slag and melt. Therefore, raising the refining temperature is beneficial not only for the wetting of inclusions by the flux but also for separating the flux and the melt.

5 Conclusions

(1) Flux purification significantly mitigates Li element loss during the Mg−9Li−3Al−1Zn alloy smelting. The refining flux creates a protective surface layer that minimizes Li oxidation and evaporation.

(2) Flux composition is crucial in determining the volume fraction of inclusions, with CaF_2 content playing a pivotal role in controlling flux viscosity and flowability. Additionally, refining temperature influences inclusion size, where higher temperatures reduce flux viscosity, enhancing the separation of slag and melt.

(3) The ideal ternary flux composition is LiCl:LiF:CaF_2 at a mass ratio of 3:1:2. The recommended refining conditions are 3% flux addition, 720 °C refining temperature, and a 10 min holding time.

(4) While flux purification does not significantly alter hardness, yield strength, or tensile strength, it remarkably enhances elongation. The refined alloy shows a substantial increase in elongation, up to 16.2%, compared to just 2.3% in the unrefined alloy. However, its effect on strength is not significant.

CRediT authorship contribution statement

Jia-wei SUN: Conceptualization, Methodology, Investigation, Formal analysis, Writing − Original draft; **Shi-hao XU:** Investigation, Writing − Review & editing; **Yu-chuan HUANG:** Writing − Review & editing, Validation; **Lian-mei WU:** Resources, Funding acquisition; **Guo-hua WU:** Supervision; **Wen-xia HU** and **Fei LI:** Writing − Review & editing; **Wen-cai LIU:** Supervision, Project administration, Funding acquisition.

Declaration of competing interest

The authors declare that they have no known competing financial interests or personal relationships that could have appeared to influence the work reported in this paper.

Acknowledgments

This study was financially supported by the National Defense Basic Research Program, China (No. JCKY2023204A005), Foundation Strengthening Plan Technical Field Fund, China (No. 2021-JJ-0112), Major Scientific and Technological Innovation Project of Luoyang, China (No. 2201029A), and the National Natural Science Foundation of China (No. U2037601).

References

[1] WU Rui-zhi, YAN Yong-de, WANG Gui-xiang, MURR L E, HAN Wei, ZHANG Zhong-wu, ZHANG Mi-lin. Recent progress in magnesium-lithium alloys [J]. International Materials Reviews, 2015, 60(2): 65−100.

[2] PENG Xiang, LIU Wen-cai, WU Guo-hua, JI Hao, DING Wen-jiang. Plastic deformation and heat treatment of Mg−Li alloys: A review [J]. Journal of Materials Science &

Technology, 2022, 99: 193−206.

[3] TIAN Guang-yuan, WANG Jun-sheng, XUE Cheng-peng, WANG Shuo, YANG Xing-hai, SU Hui, LI Quan, LI Xing-xing, YAN Cheng-ming, YANG Zhi-hao. Improving corrosion resistance of Mg−Li alloys by Sn microalloying [J]. Journal of Materials Research and Technology, 2023, 26: 199−217.

[4] PENG Xiang, SUN Jia-wei, LIU Hong-jie, WU Guo-hua, LIU Wen-cai. Microstructure and corrosion behavior of as-homogenized and as-extruded Mg−*x*Li−3Al−2Zn−0.5Y alloys (*x*=4, 8, 12) [J]. Transactions of Nonferrous Metals Society of China, 2022, 32(1): 134−146.

[5] LIU Zhan, NIE Jin-feng, ZHAO Yong-hao. Effect of deformation processing on microstructure evolution and mechanical properties of Mg−Li alloys: A review [J]. Transactions of Nonferrous Metals Society of China, 2024, 34(1): 1−25.

[6] WANG Dan, LIU Shu-juan, WU Rui-zhi, ZHANG Shun, WANG Yang, WU Hua-jie, ZHANG Jing-huai, HOU Le-gan. Synergistically improved damping, elastic modulus and mechanical properties of rolled Mg−8Li−4Y−2Er−2Zn−0.6Zr alloy with twins and long-period stacking ordered phase [J]. Journal of Alloys and Compounds, 2021, 881: 160663.

[7] YANG Yan, XIONG Xiao-ming, CHEN Jing, PENG Xiao-dong, CHEN Dao-lun, PAN Fu-sheng. Research advances of magnesium and magnesium alloys worldwide in 2022 [J]. Journal of Magnesium and Alloys, 2023, 11(8): 2611−2654.

[8] JOOST W J, KRAJEWSKI P E. Towards magnesium alloys for high-volume automotive applications [J]. Scripta Materialia, 2017, 128: 107−112.

[9] MA Chun-hui, MA Xiu-li, PEI Xing, XU Yuan-li, PENG Peng, WANG Ning. Effect of rolling reduction on the microstructure and mechanical properties of hot-rolled Mg−Li−Al−Ca alloys [J]. Materials Today Communications, 2023, 37: 107469.

[10] LI Jin-sheng, HU Hao, WANG Jun-li, FENG Zhong-xue, LI Ling-xiao, XUE Bao-shuai. Improving the microstructure and mechanical properties of ultralight Mg−Li−Zn alloy by multidirectional asymmetric rolling [J]. Materials Today Communications, 2023, 37: 107266.

[11] QIAO De-gao, DONG Shi-wen, CHEN Cui, PENG Peng, PEI Xing, YANG Xian-tao, ZHENG Wan-chao, ZHANG Hong, WANG Jia-tai. Investigation on microstructure evolution and mechanical properties of Mg−Li−Al−Ca alloy after a series of heat treatments [J]. Journal of Materials Research and Technology, 2023, 24: 1162−1176.

[12] WEI Zhen, ZHANG Jing-huai, BAO Ri-rong, WU Rui-zhi, ZHANG Hao. Achieving high strength in a Mg−Li−Zn−Y alloy by *α*-Mg precipitation [J]. Materials Science and Engineering: A, 2022, 846: 143272.

[13] ZHAO Jiong, ZHANG Jie, LIU Wen-cai, WU Guo-hua, ZHANG Liang. Effect of Y content on microstructure and mechanical properties of as-cast Mg−8Li−3Al−2Zn alloy with duplex structure [J]. Materials Science and Engineering: A, 2016, 650: 240−247.

[14] LI C Q, LIU X, DONG L J, SHI B Q, TANG S, DONG Y, ZHANG Z R. Simultaneously improved mechanical strength and corrosion resistance of Mg−Li−Al alloy by solid solution treatment [J]. Materials Letters, 2021, 301: 130305.

[15] CHEN Hao, ZHANG Meng, KONG Fan-xiao, LI Bin, CUI Xiao-fei, HUANG Yuan-ding, HORT N, WILLUMEIT-RÖMER R, XIE Wei-dong, Wei Guo-bing. Effect of extrusion and rotary swaging on the microstructural evolution and properties of Mg−5Li−5.3Al−0.7Si alloy [J]. Materials Science and Engineering: A, 2023, 885: 145627.

[16] PENG Xiang, LIU Wen-cai, WU Guo-hua. Effects of Li content on microstructure and mechanical properties of as-cast Mg−*x*Li−3Al−2Zn−0.5Y alloys [J]. Transactions of Nonferrous Metals Society of China, 2022, 32(3): 838−849.

[17] SUN Yu-hua, ZHANG Fan, WANG Ri-chu, PENG Chao-qun, REN Jian, SONG Guang-sheng. Improving the corrosion resistance of Mg−8Li−3Al−2Zn alloy by combining Gd alloying and hot extrusion [J]. Journal of Alloys and Compounds, 2023, 964: 171205.

[18] JI Hao, WU Guo-hua, LIU Wen-cai, SUN Jiang-wei, DING Wen-jiang. Role of extrusion temperature on the microstructure evolution and tensile properties of an ultralight Mg−Li−Zn−Er alloy [J]. Journal of Alloys and Compounds, 2021, 876: 160181.

[19] ZHAO De-chuan, WU Guo-qing. Effects of remelting and refining on the microstructure and properties of particle reinforced magnesium-lithium matrix composites [J]. Materials Science and Engineering: A, 2020, 788: 139607.

[20] AARSTAD K. Protective films on molten magnesium [D]. Norway: Norwegian University of Science and Technology, 2004.

[21] CAO Han-xue, HUANG Meng-tao, WANG Cheng-cheng, LONG Si-yuan, ZHA Ji-li, YOU Guo-qiang. Research status and prospects of melt refining and purification technology of magnesium alloys [J]. Journal of Magnesium and Alloys, 2019, 7(3): 370−380.

[22] PATEL S M, PATEL M M, RAO V J. Synthesis and characterization of magnesium melting fluxes [J]. Materials Research Express, 2021, 8(11): 116503.

[23] GAN Yi, HU Li, SHI Lai-xin, CHEN Qiang, LI Ming-ao, ZHOU Tao. Effect of AlLi phase on deformation behavior and dynamic recrystallization of Mg−Li alloy during hot compression [J]. Transactions of Nonferrous Metals Society of China, 2023, 33(5): 1373−1384.

[24] JI Hao, WU Guo-hua, LIU Wen-cai, ZHANG Xiao-long, ZHANG Liang, WANG Ming-xu. Origin of the age-hardening and age-softening response in Mg−Li−Zn based alloys [J]. Acta Materialia, 2022, 226: 117673.

[25] LUO A A. Magnesium casting technology for structural applications [J]. Journal of Magnesium and Alloys, 2013, 1(1): 2−22.

[26] MENG Xiang-rui, WU Rui-zhi, ZHANG Mi-lin, WU Li-bin, CUI Chong-liang. Microstructures and properties of superlight Mg−Li−Al−Zn wrought alloys [J]. Journal of Alloys and Compounds, 2009, 486(1): 722−725.

[27] OJOVAN M I, TRAVIS K P, HAND R J. Thermodynamic parameters of bonds in glassy materials from viscosity−temperature relationships [J]. Journal of Physics: Condensed Matter, 2007, 19(41): 415107.

熔剂净化对 Mg−9Li−3Al−1Zn 合金成分、显微组织和力学性能的影响

孙家伟[1]，徐仕豪[1]，黄玉川[1]，武练梅[2]，吴国华[1]，胡雯霞[2]，李 霏[2]，刘文才[1]

1. 上海交通大学 材料科学与工程学院，
轻合金精密成型国家工程研究中心和金属基复合材料全国重点实验室，上海 200240；
2. 北京电子工程总体研究所，北京 100854

摘 要：采用正交实验设计，系统研究精炼熔剂成分、精炼时间、精炼温度和熔剂添加量对 Mg−9Li−3Al−1Zn 合金显微组织和力学性能的影响。优化 Mg−Li 合金的熔剂净化工艺，并确定最有效的三元熔剂成分。结果表明，精炼熔剂通过形成保护层，显著减轻了冶炼过程中锂的损失，减少了锂的氧化和挥发。设计出的最佳熔剂成分为 m(LiCl)∶m(LiF)∶m(CaF_2)=3∶1∶2，熔剂添加量为 3%，精炼温度为 720 ℃，保温时间为 10 min。精炼后，合金的伸长率提高到 16.2%，而强度提升则较为有限。

关键词：Mg−Li 合金；熔剂净化；精炼工艺；显微组织；力学性能

(Edited by Xiang-qun LI)